Preprints of the 21st IFAC World Congress (Virtual)
Berlin, Germany, July 12-17, 2020

Reachability-Based Collision Recovery Strategy of a Quadrotor ⋆

Binbin Li * **Lei Ma** * **Duo Wang** * **Yongkui Sun** *

* *School of Electrical Engineering, Southwest Jiaotong University, Chengdu 610031,China (e-mail: bk20123885@my.swjtu.edu.cn;malei@swjtu.edu.cn; yj2019200454@my.swjtu.edu.cn;yksun@swjtu.edu.cn.)*

Abstract: Collisions with surrounding objects pose huge threat to flying quadrotors, especially in unknown environments. Unfortunately, quadrotors equipped with sensors (cameras, radars, etc.) cannot effectively detect small objects such as wires and branches. In this paper, a global stability control strategy is proposed for collision recovery based on the reachability theory. Reachability analysis is used to divide the collision recovery process into three modes:1)collision, 2)idling, 3)recovery. Safe switching conditions between different modes are generated by using solution of the Hamilton – Jacobi equation. A safe control law is presented based on the quaternion, which is proven to be globally stable and can quickly recovered from any attitude. Feasibility and performance of the proposed method are verified by experiments with collision maneuvers.

Keywords: Tele-robotics,Reachability analysis,Collision recovery,Traffic control systems.

1. INTRODUCTION

Applications of multi-rotor aircraft progressively expanding into more complex nature and urban environments (Honig et al. (2018),Nguyen et al. (2018)). Despite the remarkable progresses, motion of quadrotors is still drastically constrained by the surrounding environment. The main limitation of aircraft operation is the environment with multiple potentially colliding objects. The mainstream method for adapting to a cluttered environment is to use sensors to detect obstacles in advance(Alonso-Mora et al. (2015)). It is a common method to use high-precision on-board sensors to build accurate obstacle maps(Weiss et al. (2011)). But the obstacle detection system have functional limitations, that small objects such as wires and branches cannot be detected by sensors(cameras, radars, etc.) effectively.

Collision recovery is an necessary and vital approach to deal with aircraft impact. It attempts to adapt with impact rather than to avoid it. In practice, standard multirotor platforms are often unable to sustain flight after colliding with obstacles, because the disturbance leads to a crash. To avoid this case, a quadrotor equipped with protective covers with colliding at a low speed, can be bounced away safely. However, in the case of high-speed collisions, the aircraft will be subjected to greater impulsive interference, and more unpredictable situations will occur. The ability to recover from a collision is significant for the aircraft to perform more complex tasks. The collision recovery strategy aims to achieve stable control after the collision of the aircraft. External wrench estimation has proven to have good consequent in collision recovery, where the researchers showed a successful reflex away from a obstacle after an impact at 1.5m/s (Tomic and Haddadin (2014)). A recovery strategy combining fuzzy logic and active attitude control has been shown to have a high recovery success rate at collision speeds of up to 2m/s and inclination angles up to 17°(Dicker et al. (2017)). In the literature Battiston et al. (2017), various attitude estimation algorithms and adaptive algorithms are studied, and the performance of different algorithms in dealing with collisions is compared.

Fig. 1. Quadrotor platform.

In fact, collision recovery is a large-angle maneuver control problem. Collision recovery and the backflip maneuver has very strict requirements on the dynamic response speed of the control system. In order to solve the precise control problem of the controller action time, the method of

⋆ This work is supported by the National Natural Science Foundation of China under Grant U1730105.

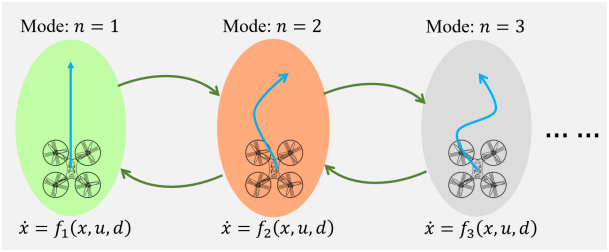

Fig. 2. An example of a hybrid system model: $n \in N$ represent discrete system, the blue arrow represents the trajectory of each mode, the green arrow represents the switch between different modes.

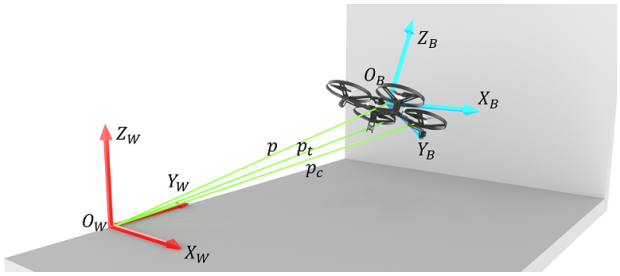

Fig. 3. Schematic diagram of collision contact model: the read frame represents world frame, and the blue frame represents body-fixed frame.

reachability-based hybrid system is adopted(Gillula et al. (2011)).

In this paper, the collision characteristics of a quadrotor and the collision recovery control strategy are studied. The collision process is divided into three modes:1)collision, in which the quadrotor impact with collision 2)idling, where the quadrotor freely rotates and falls, 3)recovery, which brings the quadrotor to a stable attitude. The reachable set of each mode is calculated by the Hamilton − Jacobi method, which provides a boundary conditions for the switching of different modes. The backflip of the quadrotor is also divided into three different modes by Ding et al. (2011). Different from the literature Ding et al. (2011), the motors does not stop working in the idling mode, which can improve the dynamic response speed of the quadrotor. And then, a quaternion-based attitude control strategy was proposed. In the experiment, the trajectory of the quadrotor is collected by the OptiTrack motion capture system(Campbell et al. (2012)) to analyze its flight characteristics. Finally, four sets of collision experiments were used to study the collision characteristics and verify the effectiveness of the collision recovery strategy.

The paper is organized as follows. Section II introduces the concept of hybrid system and the calculation method of reachable set. Section III presents the mathematical model and collision recovery maneuver. And then, a quaternion-based control strategy is presented in Section IV. The experimental results are presented in Section V, and the paper is concluded in section VI.

2. REACHABILITY CALCULATION

2.1 Hybrid Systems Model

To ensure the stability and security of complex nonlinear systems, hybrid systems are used to analyze such problems. It can decompose a nonlinear system into multiple discrete modes, each mode corresponding to a continuous dynamic model. As illustrated in Fig.2, hybrid systems consist of continuous systems(n-dimensional Euclidean space $\mathbb{R}^n$) and discrete systems(N). For any given modes i, the dynamic model can be written as

$$\dot{\boldsymbol{x}} = f(t, \boldsymbol{x}, \boldsymbol{u}, \boldsymbol{d}) \tag{1}$$

where t represents time, $\boldsymbol{x} \in \mathbb{R}^n$ represents system state of a hybrid system, $\boldsymbol{u} \in U$ represents the control input, and $\boldsymbol{d} \in D$ represents the disturbance input.

2.2 Hamilton-Jacobi Reachable Sets

The reachable sets in this work are calculated according to the Hamilton-Jacobi game formulation(see Frazzoli et al. (2005)). Let $G(t)$ denote the backwards reachable set, for any control input $\boldsymbol{u}$, the disturbance input $\boldsymbol{d}$ can drive the system into a set G_0 within time t. The boundary of the reachable set is expressed as

$$\frac{\partial \boldsymbol{J}(\boldsymbol{x}, t)}{\partial t} = -\min\{0, \max_{\boldsymbol{u}\in U} \min_{\boldsymbol{d}\in D} \frac{\partial \boldsymbol{J}(\boldsymbol{x}, t)}{\partial \boldsymbol{x}} f(t, \boldsymbol{x}, \boldsymbol{u}, \boldsymbol{d})\} \tag{2}$$

The initial undesired set G_0 is defined by the level set $\boldsymbol{J}(\boldsymbol{x}, 0) = 0$.

The capture set is defined to ensure that there is a control input that drives the system to expected state region in time t, regardless of the disturbance. The capture sets is also generated by using disturbance and the role of the control. Given by an expected target state region, the capture set can be calculated with the control input, which aims to drive the system into the desired state region and the disturbance aiming to keep the system out. Therefore, the capture set formula is the same as the avoid set formula except that the effects of input and interference are reversed. The conditions can be written as

$$\frac{\partial \boldsymbol{J}(\boldsymbol{x}, t)}{\partial t} = -\min\{0, \min_{\boldsymbol{u}\in U} \max_{\boldsymbol{d}\in D} \frac{\partial \boldsymbol{J}(\boldsymbol{x}, t)}{\partial \boldsymbol{x}} f(t, \boldsymbol{x}, \boldsymbol{u}, \boldsymbol{d})\} \tag{3}$$

It should be noted that this problem can be further simplified in the presence of the desired control law $\boldsymbol{u}(\boldsymbol{x})$. In this case, the capture set can be expressed as

$$\frac{\partial \boldsymbol{J}(\boldsymbol{x}, t)}{\partial t} = -\min\{0, \max_{\boldsymbol{d}\in D} \frac{\partial \boldsymbol{J}(\boldsymbol{x}, t)}{\partial \boldsymbol{x}} f(t, \boldsymbol{x}, \boldsymbol{u}(\boldsymbol{x}), \boldsymbol{d})\} \tag{4}$$

Security sequences for complex maneuvers can be constructed by utilizing capture and avoid sets. Starting from the final (expected) set, the backward reachable set of maneuvers is generated using the dynamics of the final£¨n-th£© maneuver in conjunction with the above mentioned attainability formulation. Then, the target area of the previous(n-1th) maneuver can be selected from the final(n-th) maneuvered capture set. Therefore, it is ensured that the initial condition in the capture set of the n-1th maneuver reaches the capture set in the n-th maneuver. This mode switching mechanism allows for safe switching to the next maneuver and ultimately safely reaches the final target set.

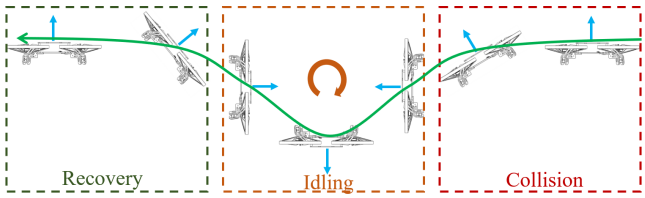

Fig. 4. The collision recovery maneuver, broken into three modes.The green arrow represents the direction of motion of the quadrotor.

3. REACHABLE SETS FOR COLLISION MANEUVER

3.1 Quadrotor Modeling

In this work, a quadrotor with four 3-D printed nylon bumpers is used for the experiment. as shown in Fig.3, the world frame $\mathscr{F}_W$ and body-fixed frame $\mathscr{F}_B$ are defined.

The relationship between the derivative of the quaternion and the quadrotor's angular velocity is expressed as

$$\dot{\mathbf{q}} = \frac{1}{2}\mathbf{q} \otimes \begin{bmatrix} 0 \\ {}^b\boldsymbol{\omega} \end{bmatrix} = \begin{bmatrix} -\frac{1}{2}\mathbf{q}_{1:3}^T \cdot {}^b\boldsymbol{\omega} \\ \frac{1}{2}(q_0\mathbf{I}_3 + [\mathbf{q}_{1:3}]_\times) \cdot {}^b\boldsymbol{\omega} \end{bmatrix} \tag{5}$$

where ${}^b\boldsymbol{\omega}$ denotes the quadrotor's body rates, and $[\mathbf{q}_{1:3}]_\times$ denotes the skew-matrix of $\mathbf{q}_{1:3}$

$$[\mathbf{q}_{1:3}]_\times = \begin{bmatrix} 0 & -q_3 & q_2 \\ q_3 & 0 & -q_1 \\ -q_2 & q_1 & 0 \end{bmatrix} \tag{6}$$

Dynamics of the quadrotor are then described by Newton-Euler equations:

$$m\ddot{\boldsymbol{p}} = m \begin{bmatrix} 0 \\ 0 \\ -g \end{bmatrix} + \mathrm{R}(\mathbf{q}_b^e)^b\boldsymbol{f} \tag{7}$$

$$\boldsymbol{\tau}_b = \boldsymbol{J}\dot{\boldsymbol{\omega}} + \boldsymbol{\omega} \times \boldsymbol{J}\boldsymbol{\omega} \tag{8}$$

where m is the total mass of the quadrotor and g is the scalar gravitational acceleration. $\mathrm{R}(\mathbf{q}_b^e)^b$ denotes the rotation quaternion that maps a vector from the body-fixed frame $\mathcal{F}_B$ to the inertial frame $\mathcal{F}_W$.

3.2 Contact Model

The schematic diagram of collision contact model is shown in Fig.3. The force F_n is applied to the fuselage at the contact point p_c can be expressed as(see Hunt and Crossley (1975))

$$F_n = \lambda\delta^n\dot{\delta} + k\delta^n \tag{9}$$

where δ represents the local deformation, λ represents damping coefficient, k represents a constant stiffness coefficient, and n represents reliance on the contact scenario. Let v_i denote the initial impact velocity, the damping coefficient can be expressed as

$$\lambda = \frac{6(1-e)}{(2e-1)^2+3}\frac{k}{v_i} \tag{10}$$

3.3 Collision Recovery Maneuver

The diagram of the collision recovery maneuver is shown in Fig.4. Without loss of generality, the collision recovery maneuver was broken into three different modes: collision mode, idling mode, and recovery mode. It should be noted that four motors of the quadrotor are not completely stopped in the idling mode, which contributes to the rapid recovery of its attitude. In the collision mode, the quadrotor turns off the output of the controller after detecting the collision. In the idling mode, the motor rotates at a low speed and the aircraft moves inertially. In the recovery mode, the controller's output is restored and the quadrotor returns to a stable state.

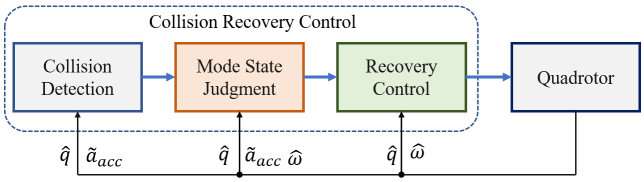

Fig. 5. Collision recovery control architecture.

In most crash situations, especially at low moving speeds, the second mode does not appear. Therefore, in this case, only the large angle maneuver recovery problem is considered, which will be introduced in Section 4. The method described in Section 2 is used to calculate the maneuver for each model. For the recovery mode, the target set was chosen as $\theta = 0 \pm 3°, \dot{\theta} = 0 \pm 15°\mathrm{s}^{-1}, \phi = 0 \pm 3°, \dot{\phi} = 0 \pm 15°\mathrm{s}^{-1}$. For the idling mode, the target set was chosen as $\theta = 110 \pm 20°, \dot{\theta} = -180 \pm s85°\mathrm{s}^{-1}, \phi = 110 \pm 20°, \dot{\phi} = -180 \pm s85°\mathrm{s}^{-1}$. For collision mode, it makes no sense to choose a target set. Because the movement of the quadrotor depends on inertia in the collision mode. The timing of switching from collision mode to idling mode can be chosen as the time that the collision occurred.

4. COLLISION RECOVERY STRATEGY DESIGN

The control task consists of three parts as shown in Fig.5. The critical control task is the large-angle maneuver control of the quadrotor. Due to the uncertainty of the attitude after the collision, the controller is required to be globally stable. The control inputs to the quadrotor are the four propeller thrust forces.

Let $\hat{\mathbf{q}}$ denote the estimated value of the attitude of the quadrotor, $\tilde{\boldsymbol{a}}_{acc}$ denote the measured values of the acceleration. The collision recovery control strategy is divided into three steps. First, it is detected whether a collision based on an estimation of its own attitude occurs or not. Then, the collision strength is estimated to determine whether the quadrotor enters the idling mode. Finally, the attitude of the quadrotor is adjusted to maintain stability.

4.1 Collision Detection

Since the aircraft collides with a vertical obstacle in a real scene, it is judged whether a collision occurs by detecting the peak of the horizontal acceleration. In the inertial frame, the acceleration of the quadrotor is obtained based on the acceleration of the body with respect to body-fixed frame and the compensation of gravity. It can be expressed as

$$\hat{\boldsymbol{a}} = \hat{\mathbf{q}} \otimes \tilde{\boldsymbol{a}}_{acc} + \boldsymbol{g} \tag{11}$$

Therefore, the collision condition is written as

$$sgn(\hat{\boldsymbol{a}}) = \begin{cases} 1 & \|[\hat{a}_x, \hat{a}_y]^{\mathbf{T}}\| > 1g \\ 0 & otherwise \end{cases} \tag{12}$$

It should be noted that the threshold of 1g still represents a very slight collision. After this collision, the quadrotor does not have to enter idling mode.

4.2 Control Law

Objective of the attitude control is to stabilize the quadrotor at arbitrarily desired angle. The commanded attitude $\mathbf{q}_{des}$ from the desired trajectory loop and the desired yaw angle have to be converted into a desired torque $\boldsymbol{\tau}_{des}$. Note that unit quaternion are not unique. That is, any physical attitude in $SO(3)$ corresponding to 2 antipodal quaternion $\pm\mathbf{q} \in \mathbb{S}^3$. If the influence of this phenomenon is neglected, quaternion-based attitude controller may cause undesirable phenomena such as unwinding, where the aerial vehicle body rotates unnecessarily through a full rotation. So, the attitude controller must satisfy

$$\boldsymbol{\omega}_{des}(\mathbf{q}) = \boldsymbol{\omega}_{des}(-\mathbf{q}) \tag{13}$$

Define a unit quaternion-based attitude tracking error

$$\mathbf{q}_{err} = \mathbf{q}^{-1} \otimes \mathbf{q}_{des} \tag{14}$$

where $\mathbf{q}$ represents the current attitude, and $\mathbf{q}_{des}$ denotes the desired attitude. The control law can be expressed as

$$\boldsymbol{\omega}_{des} = k_\tau sgn(q_{err,0}) \mathbf{q}_{err,1:3} \tag{15}$$

$$sgn(q_{err,0}) = \begin{cases} 1 & q_{err,0} \geq 0 \\ -1 & q_{err,0} < 0 \end{cases} \tag{16}$$

where k_τ denotes the tuning parameter. The sign of the quaternion error in Eq.15 is used to prevent the controller from unnecessarily commanding a rotation of more than 360 degrees.

The desired torques are computed as follows:

$$\boldsymbol{\tau}_{des} = k_r \boldsymbol{J}(\boldsymbol{\omega}_{des} - \boldsymbol{\omega}) + \boldsymbol{\omega} \times \boldsymbol{J}\boldsymbol{\omega} \tag{17}$$

where k_r is the rate controller gain, $\boldsymbol{\omega}$ is the estimated angular velocity.

Theorem 1. Thus, $\pm\mathbf{q}_{des}$ is a globally asymptotically stable equilibrium point of Eq.5.

Proof. As a first step, set $\mathbf{q}_{des} = \mathbf{q}_G$. Define an autonomous hybrid automation can be written as

$$H = (Z, Q, f, Init, Dom, E, G, R) \tag{18}$$

where $Z = z_1, z_2$ denotes two discrete states, $Q = \mathbb{S}^3 \subset \mathbb{R}^4$ denotes continuous sate $\mathbf{q}$, domains $Dom(z_1) = Dom(z_2) = \mathbb{S}^3$, edge $E = (z_1, z_2), (z_2, z_1)$, guards $G(z_1, z_2) = \{\mathbf{q} \in \mathbb{S}^3 \mid q_0 < 0\}$, reset maps $R(z_1, z_2, \mathbf{q}) = R(z_2, z_1, \mathbf{q})$, and a vector field

$$f(z, \mathbf{q}) = \begin{cases} \frac{1}{2}\mathbf{q} \otimes \mathbf{p}\big(\boldsymbol{\Omega}_{des}(z, \mathbf{q})\big), & \text{if} \quad z = z_1 \\ -\frac{1}{2}\mathbf{q} \otimes \mathbf{p}\big(\boldsymbol{\Omega}_{des}(z, \mathbf{q})\big), & \text{if} \quad z = z_2 \end{cases} \tag{19}$$

with

$$\boldsymbol{\Omega}_{des}(z, \mathbf{q}) = \begin{cases} \frac{2}{\tau}\mathbf{q}_{e,1:3} = -\frac{2}{\tau}\mathbf{q}_{1:3} & \text{if} \quad z = z_1 \\ -\frac{2}{\tau}\mathbf{q}_{e,1:3} = \frac{2}{\tau}\mathbf{q}_{1:3} & \text{if} \quad z = z_2 \end{cases} \tag{20}$$

Lyapunov function can be defined as

$$V(z, \mathbf{q}) = (1 - q_0)^2 + \mathbf{q}_{1:3}^T \mathbf{q}_{1:3} \quad \forall z \in Z \tag{21}$$

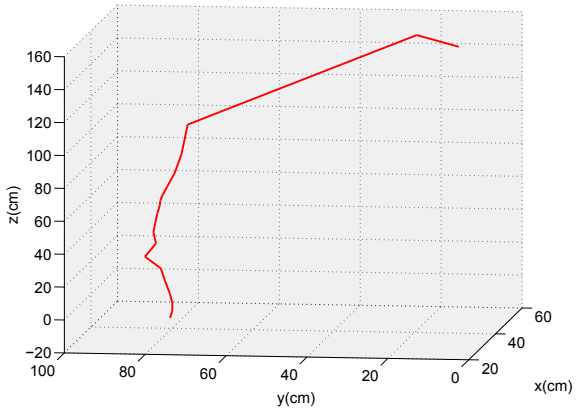

Fig. 6. Three-dimensional diagram of quadrotor collision trajectory($v_c = 0.5$m/s).

Differentiating (21) with respect to time and inserting (19) and (5) yields

$$\begin{aligned} \dot{V}(z, \mathbf{q}) &= f(z, \mathbf{q}) \frac{\partial V(z, \mathbf{q})}{\partial \mathbf{q}} \\ &= \begin{bmatrix} \frac{1}{2}\mathbf{q}_{1:3}^T \frac{2}{\tau}\mathbf{q}_{1:3} \\ -\frac{1}{2}(q_0 \mathbf{I}_3 + [\mathbf{q}_{1:3}]_\times)\mathbf{q}_{1:3} \end{bmatrix} [2(q_0 - 1) \quad 2\mathbf{q}_{1:3}^T] \\ &= -\frac{2}{\tau}\mathbf{q}_{1:3}^T (q_0 \mathbf{I}_3 + [\mathbf{q}_{1:3}]_\times)\mathbf{q}_{1:3} \\ &= -\frac{2}{\tau}\mathbf{q}_{1:3}^T \mathbf{q}_{1:3} \quad \forall z \in Z \end{aligned} \tag{22}$$

Note that

$$V(z, \mathbf{q}) > 0 \quad \forall \mathbf{q}, (z, \mathbf{q}) \in Dom(z) \setminus \{\mathbf{q}_G\} \tag{23}$$

$$\dot{V}(z, \mathbf{q}) = f(z, \mathbf{q}) \frac{\partial V(z, \mathbf{q})}{\partial \mathbf{q}} \leq 0 \quad \forall \mathbf{q}, (z, \mathbf{q}) \in Dom(z) \tag{24}$$

According to Lyapunovs stability theory, the attitude $\mathbf{q}_G$ is a globally asymptotically stable equilibrium point.

5. EXPERIMENTAL RESULT

In this section, four collision experiment results are presented. In the first and the second experiments, the trajectory and attitude of the collision between low and high speed of the quadrotor are studied respectively. In the two latter experiments, the collision recovery control strategy of the quadrotor in the case of high and low speed collision are verified, respectively.

5.1 Experiment Platform

OptiTrack motion capture system is used to capture the real-time trajectory and attitude information of the quadrotor. Optical motion capture has two advantages: (i)the optical motion capture system has a shooting speed at at least 100 FPS, (ii) the optical motion capture system has a position accuracy of 0.1 mm, A quadrotor equipped with four 3D printed nylon shields was chosen to test, as shown in Fig.1. The fuselage's body is made of carbon fiber, which guarantees strength while making it light. The total weight of the quadrotor with a 2300maH lithium

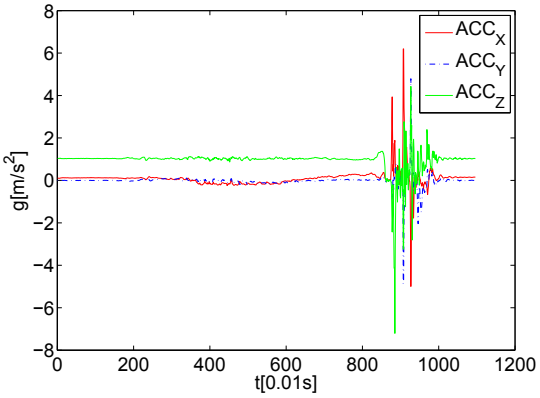

Fig. 7. Quadrotor three-axial acceleration real-time value($v_c = 0.5$m/s).

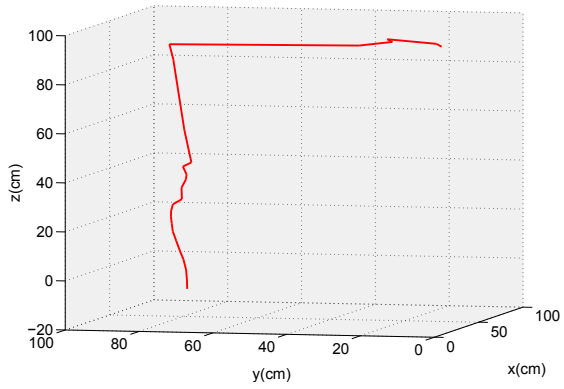

Fig. 8. Three-dimensional diagram of quadrotor collision trajectory($v_c = 2.0$m/s).

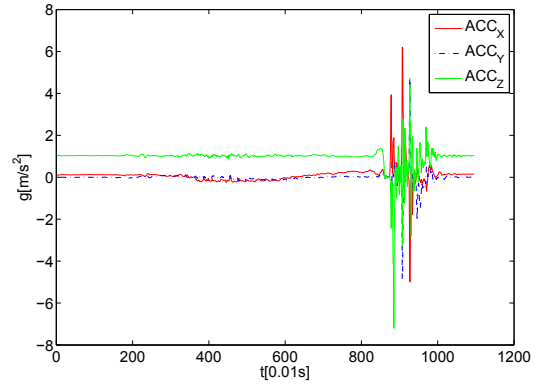

Fig. 9. Quadrotor three-axial acceleration real-time value($v_c = 2.0$m/s).

battery(4s) equipped is 0.536Kg. The powertrain uses four EMAX RS2306 motors with 5-inch blades and each motor produces a maximum thrust of 1728g.

5.2 Collision Researches

When the aircraft impacts with an obstacle, both the contact position and the contact speed have an effect on the collision result. In the first experiment, the quadrotor was controlled to hit the obstacle at a speed of 0.5m/s.

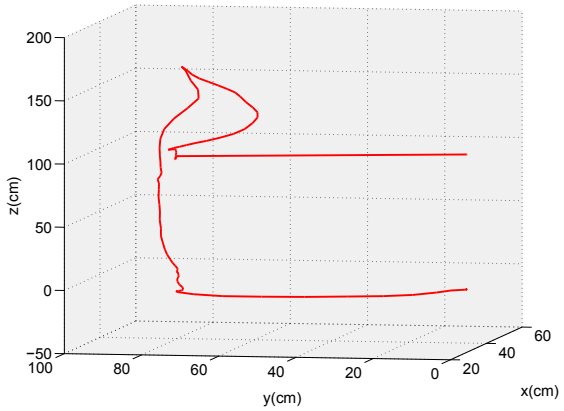

Fig. 10. Three-dimensional trajectory of collision recovery ($v_c = 0.5$m/s).

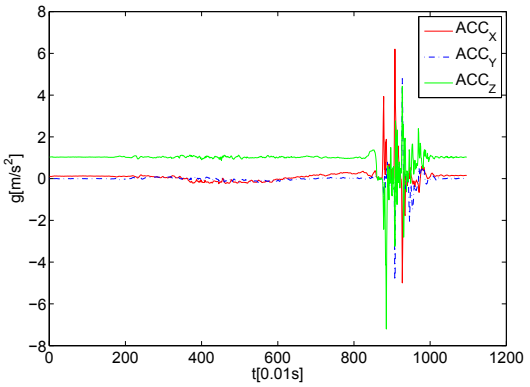

Fig. 11. Three-axial acceleration real-time value of collision recovery($v_c = 0.5$m/s).

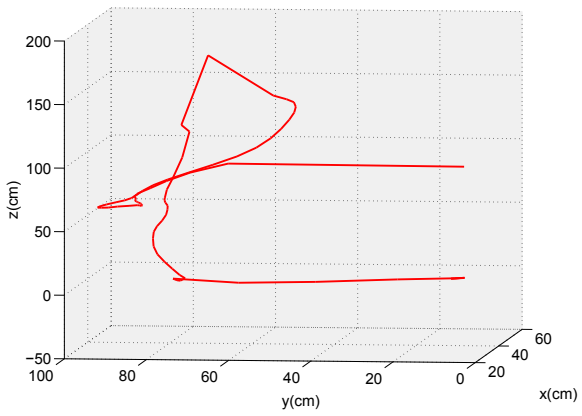

Fig. 12. Three-dimensional trajectory of collision recovery($v_c = 2.0$m/s).

The schematic diagram of the trajectory is shown in Fig.6. The real-time value of the three-axis acceleration of the quadrotor is shown in Fig.7. In the second experiment, the quadrotor was controlled to hit the obstacle at a speed of 2.0m/s. The schematic diagram of the trajectory is shown in Fig.8. The real-time value of the three-axis acceleration of the quadrotor is shown in Fig.9. Therefore, the greater speed at the time of collision makes the collision reaction

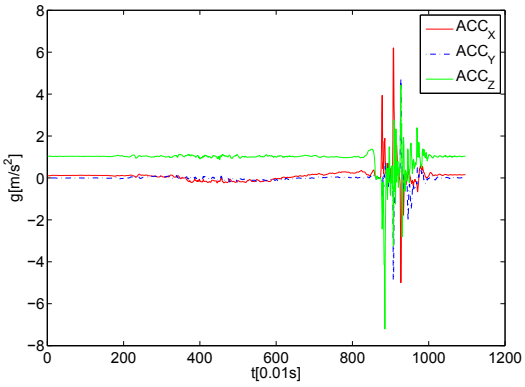

Fig. 13. Three-axial acceleration real-time value of collision recovery($v_c = 2.0$m/s).

more intense. In the second experiment, the quadrotor flipped in the air after the collision repeatedly.

5.3 Collision Recovery Research

In the third experiment, the aircraft was controlled to fly at a speed of 0.5 m/s and then hit the obstacle. The recovery trajectory of the aircraft is shown in Fig.10. In the fourth experiment, the aircraft was controlled to fly at a speed of 2.0 m/s and then hit the obstacle. The recovery trajectory of the aircraft is shown in Fig.12. Fig.11 and Fig.13 show the three-axial acceleration real-time value of collision recovery processes. In the third experiment, after the collision occurred, the fuselage of the aircraft was tilted at a large angle and then immediately returned to equilibrium. In the fourth experiment, when the collision occurred, the quadrotor rolled over 180° in the air, and then the aircraft immediately returned to equilibrium. Fig.14 illustrates the change in attitude of the quadrotor during collision recovery.

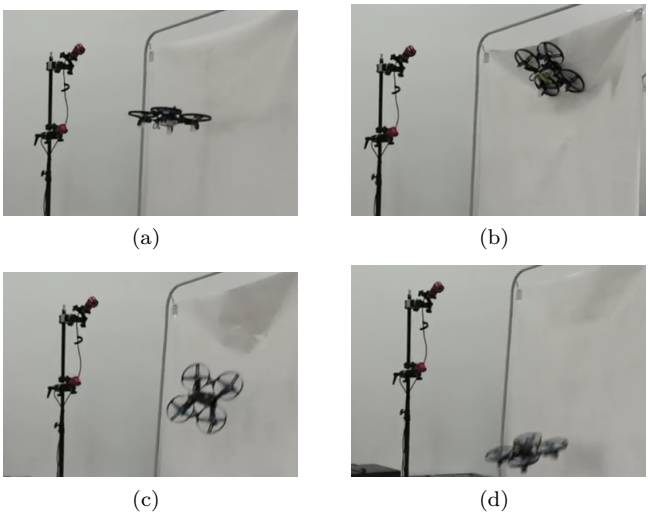

(a) (b) (c) (d)

Fig. 14. Quadrotor recovering from a collision with a vertical obstacle($v_c = 0.5$m/s): (a)the quadrotor approaching obstacles, (b)the quadrotor impacts with obstacles, (c) the quadrotor freely rotates and falls, (d)the quadrotor returns to a stable attitude.

6. CONCLUSION

A quaternion-based collision recovery strategy was proposed and the global stability of the controller was demonstrated. The experimental results show that the quadrotor can still recover a stable attitude when the collision speed is 2m/s. Future work includes testing recovery strategies under more complex conditions, which is benefits to special inspections and search and rescue applications.

REFERENCES

Alonso-Mora, J., Naegeli, T., Siegwart, R., and Beardsley, P. (2015). Collision avoidance for aerial vehicles in multi-agent scenarios. *Autonomous Robots*, 39. doi: 10.1007/s10514-015-9429-0.

Battiston, A., Sharf, I., and Nahon, M. (2017). Attitude estimation for normal flight and collision recovery of a quadrotor uav. In *2017 International Conference on Unmanned Aircraft Systems (ICUAS)*, 840–849.

Campbell, J., Hamilton, J., Iskandarani, M., and Givigi, S. (2012). A syste ms approach for the development of a quadrotor aircraft. In *2012 IEEE International Systems Conference SysCon 2012*, 1–7.

Dicker, G., Chui, F., and Sharf, I. (2017). Quadrotor collision characterization and recovery control. In *2017 IEEE International Conference on Robotics and Automation (ICRA)*, 5830–5836.

Ding, J., Gillula, J., Huang, H., Vitus, M., and Tomlin, C. (2011). Hybrid systems in robotics. *IEEE Robotics &amp amp amp Automation Magazine*, 18, 33–43. doi: 10.1109/MRA.2011.942113.

Frazzoli, E., Dahleh, M., and Feron, E. (2005). Maneuver-based motion planning for nonlinear systems with symmetries. *IEEE Transactions on Robotics*, 21, 1077–1091.

Gillula, J., Hoffmann, G., Huang, H., Vitus, M., and Tomlin, C. (2011). Applications of hybrid reachability analysis to robotic aerial vehicles. *I. J. Robotic Res.*, 30, 335–354. doi:10.1177/0278364910387173.

Honig, W., Preiss, J., Kumar, T., Sukhatme, G., and Ayanian, N. (2018). Trajectory planning for quadrotor swarms. *IEEE Transactions on Robotics*, 34, 1–14. doi: 10.1109/TRO.2018.2853613.

Hunt, K. and Crossley, F. (1975). Coefficient of restitution interpreted as damping in vibroimpact. *ASME J. Applied Mech.*, 440–445. doi:10.1115/1.3423596.

Nguyen, H.N., Park, S., Park, J., and Lee, D. (2018). A novel robotic platform for aerial manipulation using quadrotors as rotating thrust generators. *IEEE Transactions on Robotics*, 34, 353–369. doi: 10.1109/TRO.2018.2791604.

Tomic, T. and Haddadin, S. (2014). A unified framework for external wrench estimation, interaction control and collision reflexes for flying robots. *IEEE International Conference on Intelligent Robots and Systems*, 4197–4204. doi:10.1109/IROS.2014.6943154.

Weiss, S., Scaramuzza, D., and Siegwart, R. (2011). Monocular-slam-based navigation for autonomous micro helicopters in gps-denied environments. *J. Field Robotics*, 28, 854–874. doi:10.1002/rob.20412.